Inorg. Chem. **2006**, *45*, 7217–7223

A Novel Layered Titanoniobate $LiTiNbO_5$: Topotactic Synthesis and Electrochemistry versus Lithium

J.-F. Colin, V. Pralong,* V. Caignaert, M. Hervieu, and B. Raveau

Laboratoire CRISMAT, UMR 6508 CNRS ENSICAEN, 6 bd Maréchal Juin, 14050 CAEN Cedex, France

Received May 10, 2006

A new layered titanoniobate, $LiTiNbO_5$, an $n = 2$ member of the $A_xM_{2n}O_{4n+2}$ family, has been synthesized using a molten salt reaction between $HTiNbO_5$ and an eutectic "LiOH/$LiNO_3$". This compound crystallizes in the $P2_1/m$ space group with $a = 6.41$ Å, $b = 3.77$ Å, $c = 8.08$ Å, and $\beta = 92°$. It exhibits $|TiNbO_5|_\infty$ layers similar to $HTiNbO_5$, but differs from the latter by a "parallel configuration" of its $|TiNbO_6|_\infty$ ribbons between the two successive layers. The topotactic character of the reaction suggests that exfoliation plays a prominent role in the synthesis of this new form. This new phase intercalates reversibly 0.8 lithium through a first-order transformation leading to a capacity of 94 mAh/g at a potential of 1.67 V vs Li/Li^+.

Introduction

Synthesized for the first time in the 1970s, the layered titanoniobate $HTiNbO_5$[1] has been the starting point of numerous investigations not only for cationic exchange or amine intercalation (for a review, see ref 2) but also for the generation of new properties such as photoluminescence,[3,4] fast proton conductivity,[5] photocatalytic activity for hydrogen,[6] dielectric properties,[7] as well as the realization of polysiloxane composites.[8] The structure of this phase,[9] which is similar to the parent phase, $KTiNbO_5$,[10] consists of octahedral layers built up of structural units of 2×2 edge-sharing octahedra forming infinite ribbons connected to each other though their corners (Figure 1a). In this way, $HTiNbO_5$ is the $n = 2$ member of the generic family $A_xM_{2n}O_{4n+2}$, whereas $Na_2Ti_3O_7$ (Figure 1b), $K_3Ti_5NbO_{14}$ (Figure 1c), and $CsTi_2NbO_7$ (Figure 1d) are the $n = 3$ members.[11−13] Remarkably, two orientations are possible for the successive octahedral layers of the $n = 3$ members; they correspond either by a simple translation (i.e., in $Na_2Ti_3O_7$)[11] or by a glide "*a*" plane (i.e., in $CsTi_2NbO_7$).[13] Curiously, no $n = 2$ member corresponding to the same orientation of the layers as in $Na_2Ti_3O_7$ has been observed to date. Such a difference may originate from various factors such as the size of the A-site cations, the alkaline ion content, and the method of synthesis. To get a better insight into this structural behavior, we have revisited the possibility of synthesizing a new layered structure starting from $HTiNbO_5$ using molten salts instead of solutions. We report herein on a $n = 2$ member, $LiTiNbO_5$, whose original layered structure is different from the $n = 2$ member $HTiNbO_5$[9] and from $Li_{2/3}H_{1/3}TiNbO_5 \cdot 5/3\ H_2O$ [14], which exhibits a layer orientation of similar to that observed for $Na_2Ti_3O_7$.

Curiously, lithium intercalation was never investigated in the $A_xM_{2n}O_{4n+2}$ family, despite the easily reducible species Ti^{4+} and Nb^{5+} and the lamellar character of the structure which suggest a possibility for lithium intercalation. On the other hand, many titanium oxides were explored on the basis of the reversibility of the Ti^{3+}/Ti^{4+} redox couple. For example, the exceptional stability of the spinel $Li_4Ti_5O_{12}$ toward lithium insertion/extraction has generated numerous

* To whom correspondence should be addressed. E-mail: valerie.pralong@ensicaen.fr.

(1) Rebbah, H.; Desgardin, G.; Raveau, B. *Mater. Res. Bull.* **1979**, *14*, 1125.
(2) Raveau, B. *Rev. Chim. Miner.* **1984**, *21*, 391.
(3) Kudo, A.; Kaneko, E. *Microporous Mesoporous Mater.* **1998**, *21*, 615.
(4) Nakato, T.; Kusunoki, K.; Yoshizawa, K.; Kuroda, K.; Kaneko, M. *J. Phys. Chem.* **1995**, *99*, 17896.
(5) Schuler, C. C. *Z. Phys. B* **1987**, *68*, 325.
(6) Takahashi, H.; Kakihana, M.; Yamashita, Y.; Yoshida, K.; Ikeda, S.; Hara, M.; Domen, K. *Phys. Chem. Chem. Phys.* **2000**, *19*, 4461.
(7) Fang, M.; Kim, C. H.; Mallouk, T. E. *Chem. Mater.* **1999**, *11*, 1519.
(8) Bruzaud, S.; Levesque, G. *Chem. Mater.* **2002**, *14*, 2421.
(9) Rebbah, H.; Pannetier, J.; Raveau, B.; *J. Solid State Chem.* **1982**, *41* (1), 57.
(10) Wadsley, A. D. *Acta Crystallogr.* **1964**, *17*, 623.
(11) Andersson, S.; Wadsley, A. D. *Acta Crystallogr.* **1961**, *14*, 1245.
(12) Hervieu, M.; Rebbah, H.; Desgardin, G.; Raveau, B. *J. Solid State Chem.* **1980**, *35*, 200.
(13) Hervieu, M.; Raveau, B. *J. Solid State Chem.* **1980**, *32*, 161.
(14) Grandin, A. Thesis, University of Caen, Caen, France, 1987.

10.1021/ic060801o CCC: $33.50
Published on Web 07/27/2006

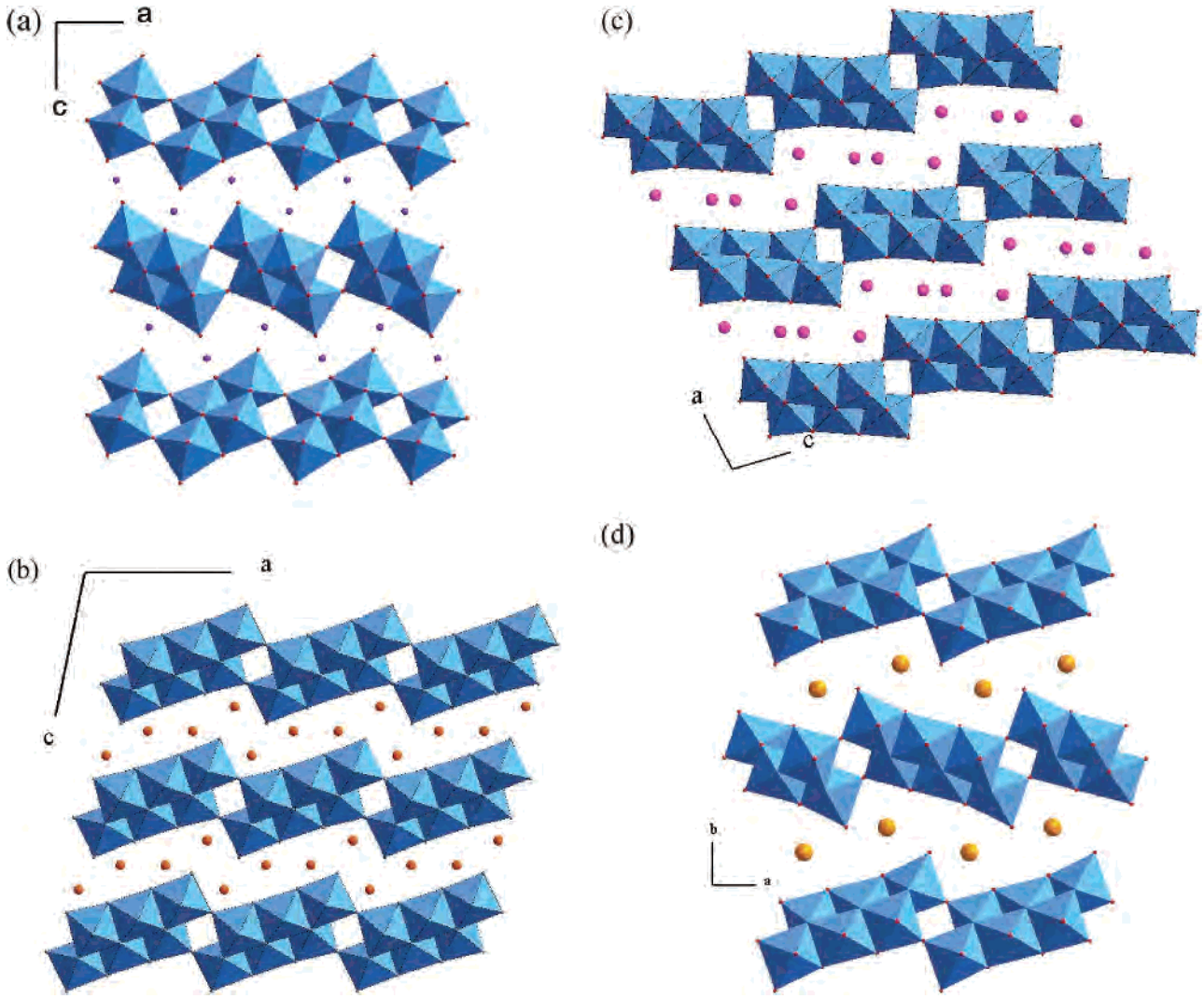

Figure 1. Structural view along the *b* axis of (a) $HTiNbO_5$ (*Pnma*, $a = 6.521(2)$ Å, $b = 3.773$ Å, $c = 16.656(4)$ Å), (b) $Na_2Ti_3O_7$ ($P2_1/m$, $a = 9.133(2)$ Å, $b = 3.806(1)$ Å, $c = 8.566(2)$ Å, $\beta = 101.57(3)°$), (c) $K_3Ti_5NbO_{14}$ ($C2/m$, $a = 18.371(6)$ Å, $b = 3.794(1)$ Å, $c = 9.199(3)$ Å, $\beta = 101.21°$), and (d) $CsTi_2NbO_7$ (*Pnma*, $a = 9.3260$ Å, $b = 18.4120$ Å, $c = 3.7980$ Å).

studies.[15] Three electrons are exchanged in a two-phase reaction at 1.52 V vs Li/Li^+ with zero polarization. In the anatase TiO_2, 0.5 lithium could be reversibly inserted at 1.83 V,[16] whereas 1.5 lithium atoms are reversibly intercalated in the ramsdellite $Li_2Ti_3O_7$ at 1.2 V.[17] Although more rare, a few studies were also devoted to the compounds with a Nb^{4+}/Nb^{5+} redox couple, as shown for $H-Nb_2O_5$, which exhibits a reversible insertion of two lithium ions at 1.6 V.[18] Thus, we have investigated the intercalation of lithium in the new $LiTiNbO_5$ phase.

Experimental Section

Chemical Synthesis. $KTiNbO_5$ was synthesized by a conventional solid-state reaction from stoichiometric amounts of K_2CO_3, Nb_2O_5, and TiO_2. The initial reagents were first mixed and preheated at 650 °C, and then the mixture was heated at 1200 °C for 12 h in a platinum crucible.

$HTiNbO_5$ was obtained from $KTiNbO_5$ by the ionic-exchange reaction. Three grams of $KTiNbO_5$ was stirred in 30 mL of a hydrochloric solution (6 N) for 3 days at room temperature. The solution was renewed three times. The white powder was then filtered and washed with distilled water until the filtrate was neutral. The X-ray powder diffraction pattern (Figure 2a) of the as prepared material, $HTiNbO_5$, corresponds to a well-crystallized phase *Pnma* with $a = 6.533(5)$ Å, $b = 3.775(3)$ Å, and $c = 16.660(1)$ Å.

For the synthesis of $LiTiNbO_5$, several attempts were made to exchange lithium for the proton via an exchange reaction between LiCl or LiBr and $HTiNbO_5$ in methanol or hexanol. Regardless of the experimental conditions, the exchange was unsuccessful. The acido-basic character of the exchange process in these phases was demonstrated by A. Grandin et al.,[14] explaining why there is no possibility of direct exchange of Li^+ from $KTiNbO_5$ phase. It is also worth noting that a low-temperature treatment of $HTiNbO_5$ is needed (<300 °C) to avoid the formation of dehydrated phase, $Ti_2Nb_2O_9$, whose appearance at 320°C from TGA analysis is not shown here.[14] Hence, $HTiNbO_5$ was mixed with an eutectic composition of 39.3 wt % LiOH and 60.7 wt % $LiNO_3$. The mixture was heated

(15) Ohzuku, T.; Ueda, A.; Yamamoto, N. *J. Electrochem. Soc.* **1995**, *142*, 1431.
(16) Peter Bruce, G. *Solid State Sci.* **2005**, *7*, 1456.
(17) Gover, R. K. B.; Tolchard, J. R.; Tukamoto, H.; Murai, T.; Irvine, J. T. S. **1999**, 146, 4348.
(18) Cava, R. J.; Murphy, D. W.; Zahurak, S. M. *J. Electrochem. Soc.* **1998**, *130* (12), 2345.

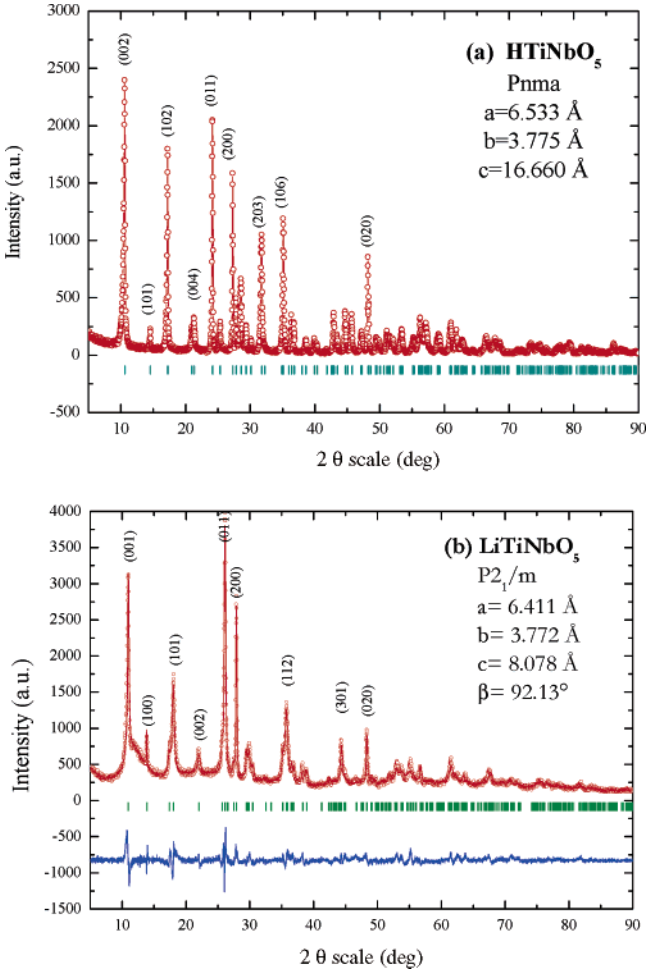

Figure 2. X-ray diffraction patterns of (a) $HTiNbO_5$ and (b) Rietveld refinement plot of X-ray diffraction data for $LiTiNbO_5$. Observed, calculated, and difference profiles are plotted on the same scale. The Bragg peaks are indicated by tick marks.

at 200 °C for 12 h. The resulting white powder was washed with water to eliminate the excess $LiOH/LiNO_3$, filtered, and dried at 60 °C.

Structural Characterizations. X-ray powder diffraction patterns (XRPD) were registered in the 2θ range of 5−120° using a Philips X'pert diffractometer with Bragg−Brentano geometry. The measurement was recorded with a 0.0167 step scan, using a Cu Kα X-ray source. The X-ray powder diffraction analysis of the air-sensitive samples was performed using an atmosphere-controlled chamber (Anton Paar TTK 450). A scanning electron microscope (SEM) Philips Field Effect Gun (FEG) XL-30 with a resolution of about 1 nm was used to study the sample morphology, while the elemental compositions were confirmed by energy dispersive spectroscopy (EDS) on a Link-Isis analyzer (ATW 6650 detector). The electron diffraction study was carried out with a JEOL 200CX transmission electron microscope (TEM) equipped with a KEVEX analyzer (energy dispersive spectroscopy). Thermogravimetric analysis (TGA) was made with a SETARAM setup in flowing argon gas. The Li content (±2%) was determined by atomic absorption analysis using a Varian spectrophotometer.

Electrochemistry. $LiTiNbO_5$ was tested as a positive electrode material in Swagelok-type cells assembled in an argon-filled glovebox with a lithium sheet (Aldrich, 1.5 mm thickness) as the negative electrode and a borosilicate glass-fiber sheet saturated with a 1 M $LiPF_6$ in ethylene carbonate (EC)/dimethyl carbonate (DMC),

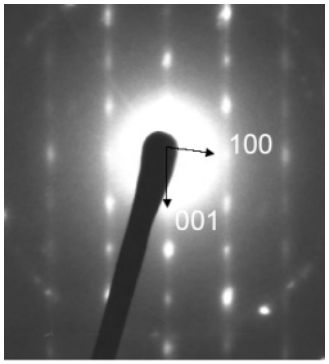

Figure 3. [010] electron diffraction patterns of $LiTiNbO_5$ showing the diffuse scattering phenomena with streaks along c^*.

1:1 w/w (LP30, Merck), as the electrolyte. The composite positive electrode was prepared by mixing the active material with 30 wt % of black carbon. The electrochemical reactivity was monitored with a VMP II potentiostat/galvanostat (Biologic SA, Claix, France). All the potentials in this paper are given versus Li/Li^+.

Results and Discussion

Structural Characterization of $LiTiNbO_5$. The EDS and atomic absorption analyses of the new phase obtained from the reaction with the eutectic lead to the composition $LiTiNbO_5$. Its X-ray powder diffraction pattern (Figure 2b) shows that this new phase, even though it is not perfectly crystallized, exhibits similarities with $HTiNbO_5$ (Figure 2a). The decrease of the c parameter from 16.6 Å for the parent phase to 8.1 Å for $LiTiNbO_5$, associated with the almost invariant a and b parameters, suggests that the new phase cannot be considered to be the result of the simple exchange of the lithium cations for protons.

The electron microscopy study evidences a lamellar morphology of the grains with a [001] preferential orientation. The [001] ED patterns are similar to those of the parent phase (i.e., $a \approx 6.4$ Å and $b \approx 3.75$ Å). The diffraction stains are sharp, suggesting that the octahedral layers built up from double-rutile-type ribbons remain unchanged. The reconstruction of the reciprocal space was carried out by tilting around the a^* and b^* axes. The existence of the diffuse scattering phenomena is observed in the reciprocal space, with streaks along c^*. On the basis of the intense nodes, the study shows a monoclinic cell with $a \approx 6.4$ Å, $b \approx 3.75$ Å, $c \approx 8.1$ Å, and $\beta \approx 92°$, without any reflection condition. One example of an [010] ED pattern is given in Figure 3. It should be noted that the streaks associated with the disorder along c^* are often more intense.

The XRPD pattern (Figure 2b) could be indexed in agreement with the ED study in a monoclinic cell with parameters $a = 6.41(1)$ Å, $b = 3.77(1)$ Å, $c = 8.08(4)$ Å, and $\beta = 92.1(2)°$. At this point, resolution of the structure was undertaken.

Despite the small size of the average crystallographic cell, a sufficient number of individualized structure factors could not be extracted to allow an ab initio structure resolution because of existence of a strong anisotropic strain and size

Table 1. Crystallographic Parameters of $LiTiNbO_5$

formula	$LiTiNbO_5$
fw	227.709
space group	$P2_1/m$
a (Å)	6.4111(3)
b (Å)	3.7717(2)
c (Å)	8.0783(6)
β (deg)	92.134(5)
V (Å^3)	195.20(2)
Z	2
ρ_{calcd} (g/cm^3)	3.871
R_{wp}	8.07
R_p	6.40
R_B	6.3

Table 2. Atomic Coordinates of $LiTiNbO_5$

atom	x	y	z	B (Å^2)	occupancy
Ti1/Nb1	0.1905(8)	1/4	0.0716(6)	1.3(3)	0.70(1)/0.30(1)
Ti2/Nb2	0.7513(7)	1/4	0.252(7)	1.6(6)	0.30(1)/0.70(1)
O1	0.078(3)	1/4	0.308(3)	2.8(6)[a]	1
O2	0.845(3)	1/4	−0.017(2)	2.8(6)	1
O3	0.439(4)	1/4	0.182(3)	2.8(6)	1
O4	0.671(3)	1/4	0.457(3)	2.8(6)	1
O5	0.260(3)	1/4	0.775(3)	2.8(6)	1

[a] The thermal factors of oxygen are constraint to the same value.

broadening of the reflections. In a first approach, a stochastic method, with the FOX software,[19] was used. The latter did not allow a suitable solution which refined all the atomic positions with accuracy to be found. However, all the solutions converged to a model in which the initial $|TiNbO_5|_\infty$ layers of the $HTiNbO_5$ structure are preserved, but two successive layers exhibit a "parallel" configuration of their structural units, as in $Na_2Ti_3O_7$ (Figure 1b). A structural model was thus elaborated, using the $P2_1/m$ space group, allowing the two crystallographic sites $(Ti, Nb)_{i=1,2}$ at the level $z = 1/4$ and $z = 3/4$ inside the same layer, as in $HTiNbO_5$. The anisotropy of the reflections was modeled with the strain-broadening formalism previously proposed by Stephens[20] and included in the FullProf program[21]. The simultaneous refinement of the profile parameters, the atomic positions, and the occupancy factors of the two sites $(Ti/Nb)_1$ and $(Ti/Nb)_2$ leads to a smaller R_I factor (10%, Table 1). The atomic positions are listed in Table 2.

These results clearly show that the structure of $LiTiNbO_5$ (Figure 4) is closely related to that of $HTiNbO_5$ (Figure 1a). It consists of similar octahedral layers built up of units of 2 × 2 edge-sharing octahedra. The latter share their apexes and edges along b, forming $|TiNbO_6|_\infty$ ribbons running along that direction. These ribbons share the corners of their octahedra along a, forming the $|TiNbO_5|_\infty$ layers. This structure differs from that of $HTiNbO_5$ in that, in two successive $|TiNbO_5|_\infty$ layers, the $|TiNbO_6|_\infty$ ribbons are parallel (Figure 4), whereas in $HTiNbO_5$, they are "antiparallel" (Figure 1a).

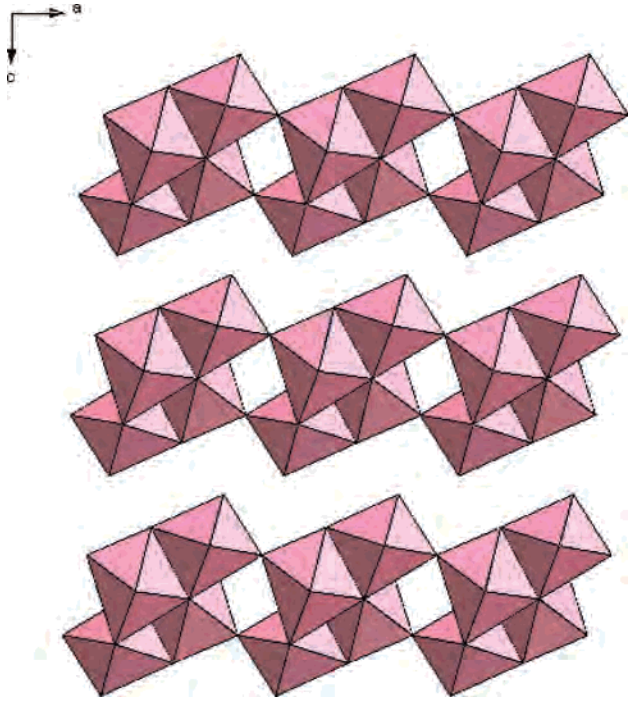

Figure 4. Structure view along b of the $LiTiNbO_5$ phase ($P2_1/m$, a = 6.4111(3) Å, b = 3.7717(2) Å, c = 8.0783(6) Å, β = 92.134(5)°).

Table 3. Interatomic Distances (Å) in $LiTiNbO_5$

	Ti	Nb
O1	2.06(6)	2.13(5)
O2	2.30(5)	2.28(5)
O2	1.95(1)	
O2	1.95(1)	
O3	1.80(6)	2.06(6)
O4		1.75(6)
O5	2.45(6)	1.90(1)
O5		1.90(1)

This change of configuration of the $|TiNbO_5|_\infty$ layers can be explained by the smaller size of the Li^+ cations. Indeed it has been observed that in the generic $A_xM_{2n}O_{4n+2}$ family, large cations, such as cesium, lead to an antiparallel configuration of the octahedral layers, as shown for $CsTi_2NbO_7$;[13] and smaller cations, such as sodium, lead to a parallel configuration, as shown for $Na_2Ti_3O_7$,[11] whereas intermediate-size cations, such as potassium, may involve both configurations (e.g., antiparallel, as in $KTiNbO_5$,[10] and parallel, as in $K_3Ti_5NbO_{14}$).[12]

The interatomic distances (Table 3) are rather similar to those observed for $HTiNbO_5$ except that the (Ti, Nb)−O distances corresponding to O_5 and O_3 seem to be unrealistic (2.45 and 1.79 Å, respectively). The location of the latter atoms, in more realistic positions does not significantly increase the reliability factor. Note also that the distribution of the titanium and niobium cations between the two octahedral sites is identical to that observed for $HTiNbO_5$.[9]

From this structural study, it appears that the integrity of the $|TiNbO_5|_\infty$ layers is preserved during the reaction between $HTiNbO_5$ and eutectic $LiOH/LiNO_3$. Moreover, the diffuse streaks observed along c^* in the ED patterns suggest that this reaction is topotactic. The topotactic process may lead,

(19) Favre-Nicolin, V.; Cerny, R. *J. Appl. Crystallogr.* **2002**, *35*, 734−743.
(20) Stephens, P. W. *J. Appl. Crystallogr.* **1999**, *32*, 281.
(21) Rodriguez-Carvajal, J. *Collected Abstracts*; Powder Diffraction Meeting, Toulouse, France, July 16−19, 1990; International Union of Crystallography: Chester, U.K., 1990; p 127.

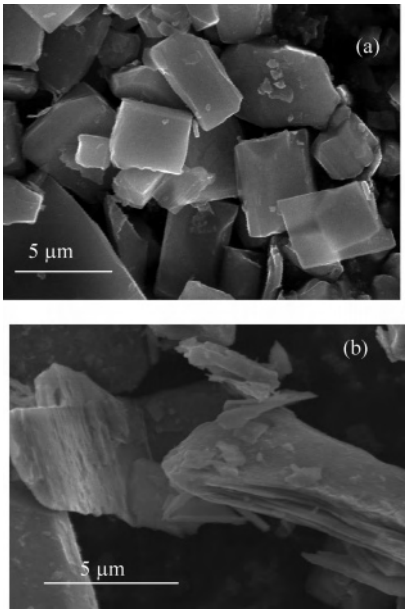

Figure 5. Scanning electron micrographs of (a) $HTiNbO_5$ and (b) $LiTiNbO_5$.

schematically, to the reorganization of one $|TiNbO_5|_\infty$ layer out of two through a complex step-by-step mechanism, such as layer gliding or block shearing, as observed in some layered structures.[22,23] Starting from $HTiNbO_5$ crystals, which are about 5 μm polyhedra (Figure 5a), the SEM images after reaction (Figure 5b) show milfoil stacking, characteristic of the exfoliation phenomena. The latter likely results from the strains released during the topotactic reaction. This also explains why the model of the anisotropic broadening of the XRPD peaks is difficult to realize and remains imperfect. The 00*l* reflections of the XRPD patterns are indeed dramatically broadened, whereas the 0*k*0 and *h*00 reflections, which characterize the layers, remain well resolved, in agreement with ED observations. These broadenings result from the great number of stacking faults of the $|TiNbO_5|_\infty$ layers along the *c* axis in the course of the step-by-step process. It is most likely that broadenings caused by the shape of the crystallites also affect the refinement of the structure, especially for the lighter oxygen atoms.

Electrochemical Behavior versus Lithium. Figure 6a reports the potentiodynamic cycling curve performed in the potential windows of 3−1 V with 10 mV potential steps once the current was lower than an equivalent *C*/300 galvanostatic regime or a step duration equal to 1 hour. This technique was first proposed by Thompson et al.[24,25] The recording the chronoamperometric responses of the system at every potential level gives access to the evolution of the kinetics for each redox level. This allows us to distinguish between a single-phase solid solution domain in which the kinetics are most often governed by diffusion laws and a two-phase domain in which the kinetics is usually governed by the mobility of the interface between the two phases,[26−28] similar to what is observed for the nucleation and growth processes.[29−32] In the enlargement (Figure 6b), we observed a bell-shapedchronoamperogram, characteristic of the progress of a first-order transformation. Such a transformation is confirmed by the narrow peak (<200 mV) observed on the derivative curve d*Q* versus volts (Figure 6c) from a *C*/10 galvanostatic cycle. The evolution of the current (Figure 6b) reflects the displacement of the interface under the overpotential from the two-phase equilibrium potential (1.67 V), with a possible evolution of its area, which usually increases at the beginning and decreases as the phase transformation is completed. For a given potential, the current is constant as a function of time during several steps with a current value proportional to ΔV and a transformation potential close to 1.67 V. This type of response is observed both in solid/solid and solid/solution transformations and characterizes a first-order transformation limited by the progress of the interface area. Then, in the potential window of 1−3 V, a reversible capacity of 1.2 lithium is obtained (i.e., a capacity of 120 mAh/g). After the first 20 cycles, the capacity fades to 0.8 lithium, but then no significant loss of capacity is measured during the 20 remaining cycles, showing a good stability upon cycling (Figure 7).

To summarize, from the electrochemical study, we find that $LiTiNbO_5$ can reversibly intercalate 0.8 lithium through a first-order transformation at 1.67 V. Even if two process are clearly evidenced on the derivative curve (Figure 6.c) at 1.55 and 1.67 V, respectively, it is worth noting that because of the random cationic distribution between Ti^{4+} and Nb^{5+}, in addition to the fact that they have similar redox potentials, we could not distinguish which couple is involved during the redox processes at 1.55 and 1.67 V. However, the crystallographic sites available for the lithium are different depending on the initial lithium location. It is therefore worth noting that no intercalation is possible in the antiparallel-type phase, $KTiNbO_5$ (not shown here), becasuse of the absence of available sites for the lithium ions. Figure 8 shows the X-ray diffraction pattern of an electrode at the end of the first discharge and charge. Upon cycling, very few changes are observed (a slight amorphization and some intensities vary), suggesting that the first discharge involves the formation of either an amorphous phase or a new phase "Li_2TiNbO_5" whose structure is closely related to the parent

(22) Fransson, L. M. L.; Vaughey, J. T.; Benedek, R.; Edström, K.; Thomas, J. O.; Thackeray, M. M. *Electrochem. Commun*. **2001**, *3*, 317.
(23) Poizot, P.; Chevallier, F.; Laffont, L.; Morcrette, M.; Rozier, P.; Tarascon, J.-M. *Electrochem. Solid State Lett.* **2005**, *8*, A184.
(24) Thompson, A. H. *J. Electrochem. Soc.* **1979**, *126*, 603.
(25) Thompson, A. H. *Rev. Sci. Instrum*. **1983**, *54*, 229.
(26) Pyun, S.-I.;Yoon, Y.-G. *Mol. Cryst. Liq. Cryst.* **1998**, *123*, 311.
(27) SacEpee, N.; Palacin, M. R.; Beaudouin, B.; Delahaye-Vidal, A.; Jamin, T.; Chabre, Y.; Tarascon, J.-M. *J. Electrochem. Soc.* **1997**, *144*, 3896.
(28) Chabre, Y. Physics of Intercalation II. *NATO ASI Ser. B* **1993**, 305, 181.
(29) Shin, H.-C.; Pyun, S. I. *Electrochim. Acta* **1999**, *44*, 2235.
(30) Philibert, J. *Atom Movement, Diffusion and Mass Transport in Solid*; Les Editions de Physique: Les Ulis, France, 1991.
(31) Sharifker, B. R.; Hills, G. J. *Electrochim. Acta* **1983**, *28*, 879.
(32) Southampton Electrochemistry Group. *Instrumental Methods In Electrochemistry*; Ellis Horwood Series in Physical Chemistry; Ellis Horwood: New York, 1985.

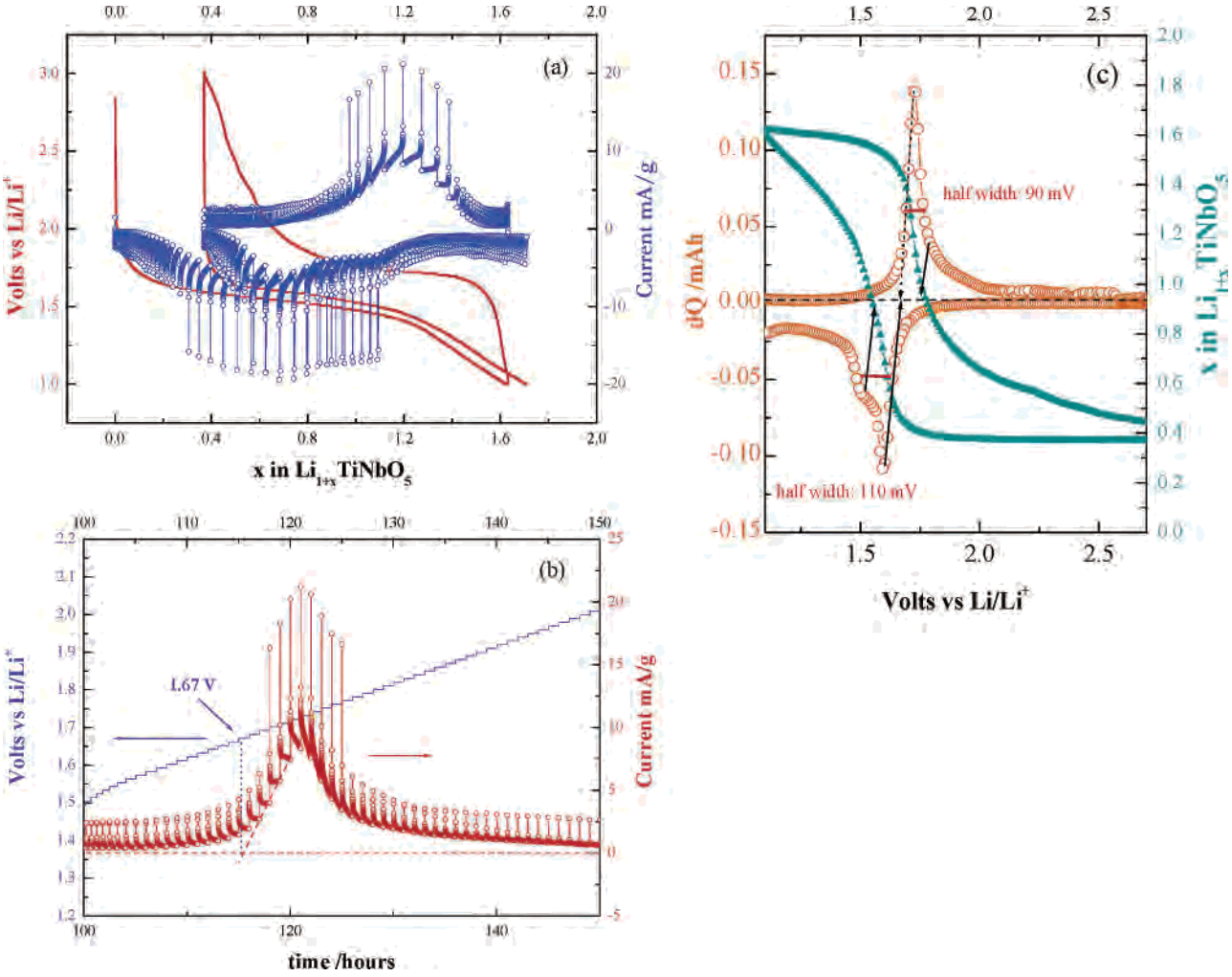

Figure 6. $LiTiNbO_5$ potential composition curves. (a) Amperometric responses (dotted lines) to 10 mV potential steps (continuous line) with stepping of the potential once the duration of the step is higher than 1 h or the current is lower than an equivalent *C*/300 galvanostatic regime. (b) Enlargement of the chronoamperometric response in the course of the first charge between 1 and 3 V. (c) derivative curve d*Q* vs the potential and the corresponding galvanostatique curve at a *C*/10 rate of the second cycle.

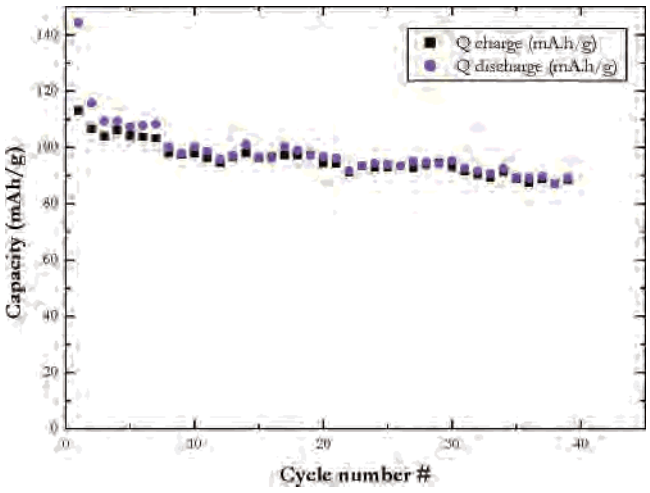

Figure 7. Capacity versus cycle number for the $LiTiNbO_5$ electrode containing 30 wt % acetylene (black). The potential window is 3−1 V.

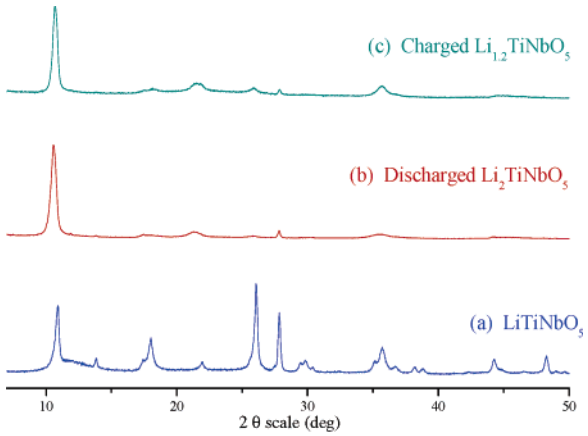

Figure 8. X-ray diffraction pattern of (a) the starting material, $LiTiNbO_5$, (b) the discharged $LiTiNbO_5$ electrode withdraws after a first discharge until 1 V, and (c) the electrochemically charged phase at 3 V.

phase $LiTiNbO_5$. The latter hypothesis is more likely because no broad peak is visible at a low-scattering angle. Further neutron diffraction studies are needed to gain a deeper understanding of this structural transformation.

Conclusion

In conclusion, a new member of the $A_xM_{2n}O_{4n+2}$ family, $LiTiNbO_5$ has been synthesized. It is the first time that such a $n = 2$ member with a parallel configuration of the $|TiNbO_6|_\infty$ octahedral ribbons is obtained. Moreover, the

lithium insertion process occurs via a first-order reaction at 1.67 V with a reversibility of 0.8 Li. The structural stability upon lithium insertion/extraction gives good reversibility in $LiTiNbO_5$. Although, the reversible capacity is small (94 mAh/g), the 1.67 V redox potential and low-temperature preparation method makes it attractive as electrode material for Li-ion batteries. The electrochemical behavior of other members of the $A_xM_{2n}O_{4n+2}$ family will be reported in a forthcoming paper.

Acknowledgment. We gratefully acknowledge the CNRS and the Minister of Education and Research for financial support through their Research, Strategic, and Scholarship programs, and the European Union for support through the network of excellence FAME.

IC060801O